Negative Thermal Expansion and Phase Transitions in the $ZrV_{2-x}P_xO_7$ Series

V. Korthuis, N. Khosrovani, and A. W. Sleight*

Department of Chemistry, Oregon State University, Corvallis, Oregon 97331-4003

N. Roberts, R. Dupree,† and W. W. Warren, Jr.

Department of Physics, Oregon State University, Corvallis, Oregon 97331-6507

Received October 4, 1994. Revised Manuscript Received November 17, 1994®

Phases in the $ZrP_{2-x}V_xO_7$ series show isotropic thermal expansion which for some members is negative over a broad temperature range up to at least 950 °C. One phase transition occurs for ZrP_2O_7 at 290 °C. The thermal expansion is normal below this transition but is very low and positive above this transition. Two phase transitions occur in ZrV_2O_7 close to 100 °C; each results in an abrupt increase in volume with increasing temperature. Strong negative thermal expansion commences in ZrV_2O_7 above 100 °C and continues to about 800 °C, where decomposition occurs. Below the phase transitions in cubic ZrP_2O_7 and ZrV_2O_7, a $3 \times 3 \times 3$ superstructure develops with no apparent change in space group. In the high-temperature structures, the V–O–V and P–O–P angles are constrained by the $Pa\bar{3}$ space group symmetry to be 180°. After the $3 \times 3 \times 3$ superstructure develops, this symmetry constraint is relaxed for some, but not all, V–O–V and P–O–P linkages. The $3 \times 3 \times 3$ superstructure results in eleven crystallographic sites for V or P. Room-temperature ^{51}V and ^{31}P NMR spectra for ZrV_2O_7 and ZrP_2O_7 show complex patterns consistent with the $Pa\bar{3}$ space group and the $3 \times 3 \times 3$ superstructure. Modeling studies suggest that the unique thermal expansion properties are related to frustration in bending V–O–V or P–O–P angles away from 180° in a cooperative manner. For the mid region of the ZrV_2O_7–ZrP_2O_7 solid solution, phase transitions above room temperature are completely suppressed. For the $ZrP_{2-x}V_xO_7$ series, ^{31}P NMR studies show a preponderance of VPO_7^{4-} groups, relative to a mixture of $V_2O_7^{4-}$ and $P_2O_7^{4-}$ groups, when x is close to 1.0. Results in the HfV_2O_7–HfP_2O_7 system are essentially identical to those in the ZrV_2O_7–ZrP_2O_7 system.

Introduction

Of the few materials showing negative volume thermal expansion, most are anisotropic.[1] During heating, their unit cells are actually expanding in some directions while they are contracting in other directions. This combination sometimes leads to a small volume contraction with increasing temperature. Examples of this phenomenon are found in $PbTiO_3$,[2] β-eucryptite ($LiAlSiO_4$),[3] $(ZrO)_2P_2O_7$,[4] and the NZP family (e.g., $NaZr_2P_3O_{12}$).[1] The rare instances of isotropic negative thermal expansion tend to occur only over a very limited temperature range. For example, negative thermal expansion is found in cubic or pseudocubic $BaTiO_3$, but only at temperatures very close to the orthorhombic-to-tetragonal and the tetragonal-to-cubic phase transitions.[5] Low negative thermal expansion is also found in some relaxor ferroelectrics close to their diffuse phase transitions.[1] Certain oxide glasses and glass ceramics show low negative thermal expansion, but only at temperatures below room temperature.[1] The ZrP_2O_7 type structure is apparently unique in providing for isotropic negative thermal expansion over a very broad temperature range.[6]

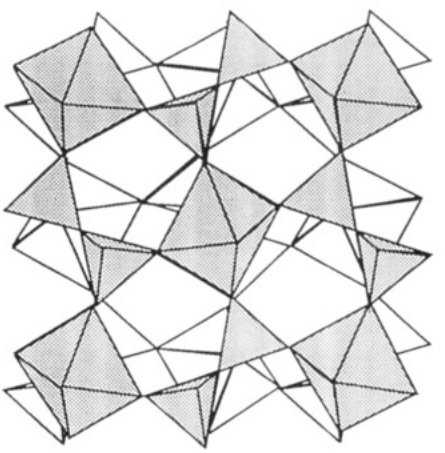

Figure 1. Ideal structure for cubic $A^{4+}M^{5+}{}_2O_7$ compounds.

A family of $A^{4+}M^{5+}{}_2O_7$ compounds exists with a cubic structure (Figure 1) which may be described by its relationship to the NaCl structure. In this description, the cation is A^{4+} and the anion is $(M_2O_7)^{4-}$. The ordered orientation of the $(M_2O_7)^{4-}$ group necessarily lowers the symmetry of the NaCl structure. The space group for NaCl is $Fm3m$ while the highest symmetry space group

† Permanent address: Department of Physics, Warwick University, Coventry CV4 7AL, U.K.

® Abstract published in *Advance ACS Abstracts,* December 15, 1994.

(1) Roy, R.; Agrawal, D. K.; McKinstry, H. A. *Annu. Rev. Mater. Sci.* **1989**, *19*, 59.
(2) Shirane, G.; Hoshino, S. *J. Phys. Soc. Jpn.* **1951**, *6*, 265.
(3) Gillery, F. H.; Bush, E. A. *J. Am. Ceram. Soc.* **1959**, *42*, 175.
(4) Harrison, D. E.; McKinstry, H. A.; Hummel, F. A. *J. Am. Ceram. Soc.* **1954**, *37*, 277.
(5) Shirane, G.; Takeda, A. *J. Phys. Soc. Jpn.* **1952**, *7*, 1.
(6) Taylor, D. *Br. Ceram. Trans. J.* **1984**, *83*, 5.

0897-4756/95/2807-0412$09.00/0

possible for this $A^{4+}M^{5+}{}_2O_7$ family is $Pa\bar{3}$. The A^{4+} cation may be Th, U, Pu, Ce, Hf, Zr, Ti, Mo, W, Re, Pb, Sn, Ge, or Si when M is phosphorous.[7-20] Double substitution on the A^{4+} site is possible leading to a family of the type $A^{3+}{}_{0.5}A^{5+}{}_{0.5}P_2O_7$ where A^{3+} may be Bi, Sb, or a rare earth metal and A^{5+} may be Nb, Ta, or Sb.[21] One form of $Sb^{3+}Sb^{5+}(P_2O_7)_2$ has a structure very closely related to that of ZrP_2O_7.[22] Certain tantalum and niobium phosphates are also known to have this basic structure type.[23] Arsenates can have the cubic ZrP_2O_7 structure when A^{4+} is Zr or Th.[24,25] The only vanadate known to have this structure is ZrV_2O_7.[26-28] At high temperatures, these compounds presumably have the ideal structure (Figure 1). However, apparently all of these compounds possess phase transitions well above room temperature. Below the phase transitions, the structures appear to remain cubic but a superstructure develops which requires tripling the cubic cell edges. The thermal expansion of $A^{4+}M^{5+}{}_2O_7$ phases might be considered normal at temperatures below the tripling phase transition. However, above this transition, the thermal expansion can be very low and can become negative. In the case of ZrV_2O_7 and HfV_2O_7, the thermal expansion is highly negative from about 150 °C up to their decomposition temperatures of about 800 °C.

A purpose of our study has been to better understand the structures, phase transitions and negative thermal expansion in certain $A^{4+}M^{5+}{}_2O_7$ phases which have the ZrP_2O_7 type structure. Another objective has been to design and prepare materials which show isotropic negative thermal expansion over a useful temperature range. Such materials are expected to find application, for example, in adjusting the thermal expansion of composites to very low values. The low thermal expansion materials based on anisotropic materials frequently show problems of microcracking during thermal cycling. This microcracking is attributed to their anisotropic character. The isotropic materials described here should, therefore, overcome this problem.

Experimental Section

Reactants used were $ZrOCl_2{\cdot}8H_2O$, $HfOCl_2{\cdot}8H_2O$, NH_4VO_3, and $(NH_4)_2HPO_4$. Two different synthesis routes were employed. One was a solid-state reaction using appropriate amounts of reactants to form various phases of the type $Zr_{1-y}Hf_yV_{2-x}P_xO_7$. In this route, the reactants were first mixed by grinding with an agate mortar and pestle. This intimate mixture was then placed in a Pt crucible and heated at 750 °C in air for 24 h. Evolution of NH_4Cl, NH_3, and H_2O occurs during the initial stages of heating. This material was then reground and heated a second time at 750 °C in air for 24 h.

The second synthesis procedure begins with two aqueous solutions. One solution contains appropriate amounts of $ZrOCl_2{\cdot}8H_2O$ and/or $HfOCl_2{\cdot}8H_2O$. The other solution contains appropriate amounts of NH_4VO_3 and/or $(NH_4)_2HPO_4$. The pH of the latter solution is brought to 2.0 by the addition of nitric acid. Both solutions are then brought to 90 °C. The Hf and/or Zr solution is added to the P and/or V solution with constant stirring. A precipitate forms immediately. After stirring for 1 h, this dispersion is dried at 120 °C for 10 h. This product is then ground and heated in a Pt crucible at 700 °C in air for 4 h.

X-ray diffraction data were obtained on a Siemens D5000 diffractometer with Cu Kα radiation using Si as an internal standard. A sample holder was constructed which allowed heating of samples to 250 °C. High-resolution neutron diffraction powder data were obtained at Brookhaven National Laboratory. A Netzch thermal analysis system was used to obtain thermal gravimetric (TGA), differential scanning calorimetry (DSC), and dilatometer data in air. The DSC data were collected over the temperature range −40 to 800 °C. Dilatometer and TGA data were taken from room temperature to 900 °C.

Nuclear magnetic resonance (NMR) with magic angle spinning (MAS) was used to study $ZrV_{2-x}P_xO_7$ samples with compositions $x = 2.0$, 1.6, 1.0, 0.3, and 0.0. Experiments were carried out using a Chemagnetics CMX360 spectrometer at a spinning frequency of 5 kHz in a magnetic field of 8 T. One spectrum was also obtained at a MAS frequency of 18 kHz in a 11.7 T field. NMR spectra were obtained for both ^{51}V and ^{31}P. The ^{51}V nucleus has a gyromagnetic ratio $\gamma = 11.19$ MHz/T, a spin $I = {}^7/_2$, and electric quadrupole moment $Q = -4 \times 10^{-2}$ barn. The ^{31}P nucleus has a $\gamma = 17.235$ MHz/T and $I = {}^1/_2$. Variable-temperature NMR in the range 25−180 °C was used to study the structural phase transitions in ZrV_2O_7.

Results

The isostructural compounds HfV_2O_7, ZrV_2O_7, HfP_2O_7, and ZrP_2O_7 were found to be completely miscible in one another. The room-temperature cubic cell edges for the $ZrV_{2-x}P_xO_7$ series are shown in Figure 2. The subcell value for a is used for all members of the series. However, a $3 \times 3 \times 3$ superstructure is observed for the end members and for compositions close to the end members.

Thermal expansion data for the $ZrV_{2-x}P_xO_7$ series are shown in Figure 3. No weight changes were detected by TGA during heating or cooling. Essentially identical results were obtained when Hf was substituted for Zr. Essentially identical results were also obtained when the same composition was prepared by different methods. The cubic cell edge for ZrV_2O_7 was also determined as a function of temperature up to 250 °C. The results agree well with the dilatometer data in Figure 3 and with previous results.[27,28] For ZrP_2O_7 and HfP_2O_7, there

(7) Laud, K. R.; Hummel, R. A. *J. Am. Ceram. Soc.* **1971**, *54*, 296.
(8) Harrison, D. E.; Hummel, R. A. *J. Am. Ceram. Soc.* **1959**, *42*, 487.
(9) Merz, K. M.; Smyth, H. T.; Kirchner, H. P.; Beal, J. L. Cornell Aeronautical Lab., Report No. PI-1273-M-8, 1960.
(10) Harrison, D. E.; McKinstry, H. A.; Hummel, F. A. *J. Am. Ceram. Soc.* **1954**, *37*, 277.
(11) Burdese, A.; Lucco Borlera, M. *Ann. Chim. Roma* **1963**, *53*, 333.
(12) Burdese, A.; Lucco Borlera, M. *Atti. Acad. Sci. Torinao. Cl. Sci. Fis. Mater. Nat.* **1959**, *94*, 107.
(13) Huang, C.-H.; Knop, O.; Othen, D. A. *Can. J. Chem.* **1975**, *53*, 79.
(14) Vö llenkle, H.; Wittman, A.; Nowotny, H. *Monatsh. Chem.* **1963**, *94*, 956.
(15) Hagman, L.-O.; Kierkegaard, P. *Acta Chem. Scand.* **1969**, *23*, 327.
(16) Liebau, F.; Bissert, G.; Koppen, N. *Z. Anorg. Allg. Chem.* **1968**, *359*, 113.
(17) Hagman, L.-O.; Kierkegaard, P. *Acta Chem. Scand.* **1969**, *23*, 327.
(18) Kinomura, N.; Hirose, M.; Kumada, N.; Muto, F. *Mater. Res. Bull.* **1985**, *20*, 379.
(19) Bjorklund, C. W. *J. Am. Chem. Soc.* **1957**, *79*, 6347.
(20) Teweldemedhin, Z. S.; Ramanujachary, K. V.; Greenblatt, M. *Mater. Res. Bull.* **1993**, *28*, 427.
(21) Oyetola, S.; Verbaere, A.; Guyomard, D.; Crosnier, M. P.; Piffard, Y.; Tournoux, M. *Eur. J. Solid State Inorg. Chem.* **1991**, *28*, 23.
(22) Verbaere, A.; Oyetola, S.; Guyomard, D.; Piffard, Y. *J. Solid State Chem.* **1988**, *75*, 217.
(23) Haider, S. Z. *Anal. Chim. Acta* **1961**, *24*, 250.
(24) Hajo, O. *Naturwissenschaften* **1965**, *52*, 344.
(25) Le Flem, G.; Lamic, J.; Hagenmuller, P. *Mémoires Présentés A La Société Chimique, June*, **1966**, 1880.
(26) Peyronel, G. *Gazz. Chim. Ital.* **1942**, *72*, 77.
(27) Craig, D. F.; Hummel, F. A. *J. Am. Ceram. Soc.* **1972**, *55*, 532.
(28) Buchanan, R. C.; Wolter, G. W. *J. Electrochem. Soc.* **1983**, *130*, 1905.

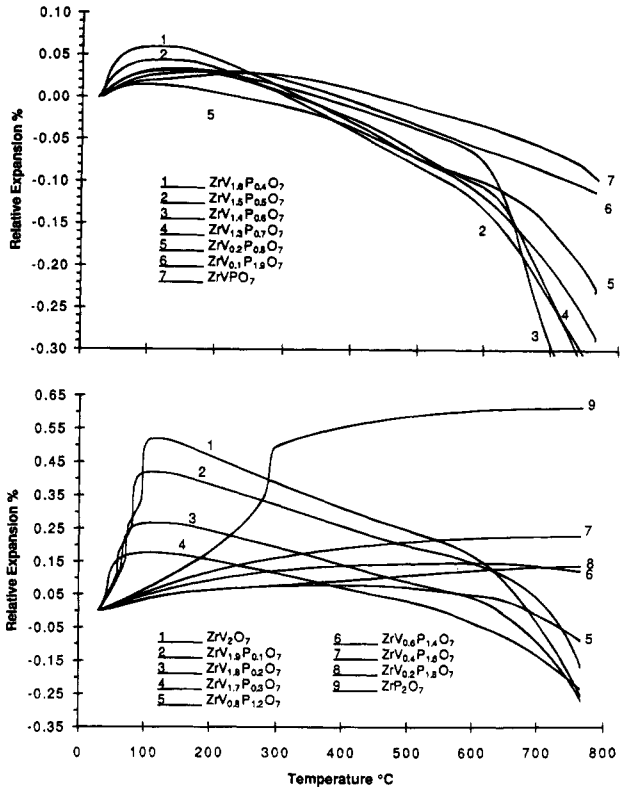

Figure 2. Unit cell edges for the $ZrV_{2-x}P_xO_7$ series based on the ideal structure.

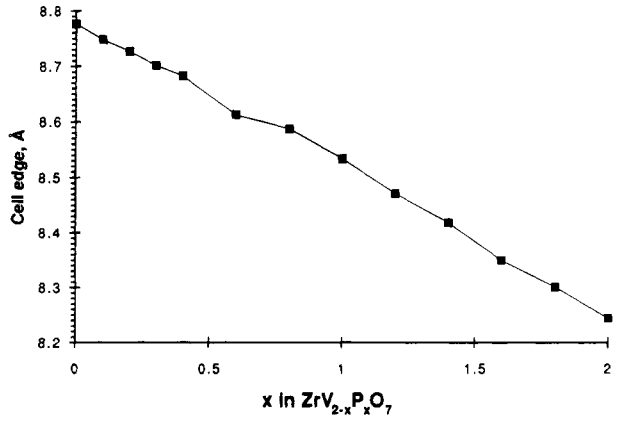

Figure 3. Thermal expansion of the $ZrV_{2-x}P_xO_7$ series based on dilatometer data.

is apparently only one phase transition close to 350 °C. However, for both ZrV_2O_7 and HfV_2O_7, there are two abrupt phase transitions close to 100 °C. The change in slope of the thermal contraction at about 600 °C is possibly indicative of another phase transition. However, our DSC results do not show any evidence for a transition near 600 °C. Furthermore, our ^{51}V NMR data indicate that the ideal structure is achieved by 130 °C.

DSC measurements on ZrV_2O_7 showed sharp transitions at 77 and 102 °C corresponding to the abrupt changes in volumes shown in Figure 3. The sharpness of these transitions and the hysteresis of these transitions indicate that they are first order. Neutron and X-ray diffraction data show a 3 × 3 × 3 superstructure below and above the 77 °C transition but no superstructure above the 102 °C transition. An attempt was made to follow both of these transitions in a $ZrV_{2-x}P_xO_7$ series. For $x = 0.1$, the two transitions dropped to 66 and 89 °C; for $x = 0.2$, the two transitions had dropped again

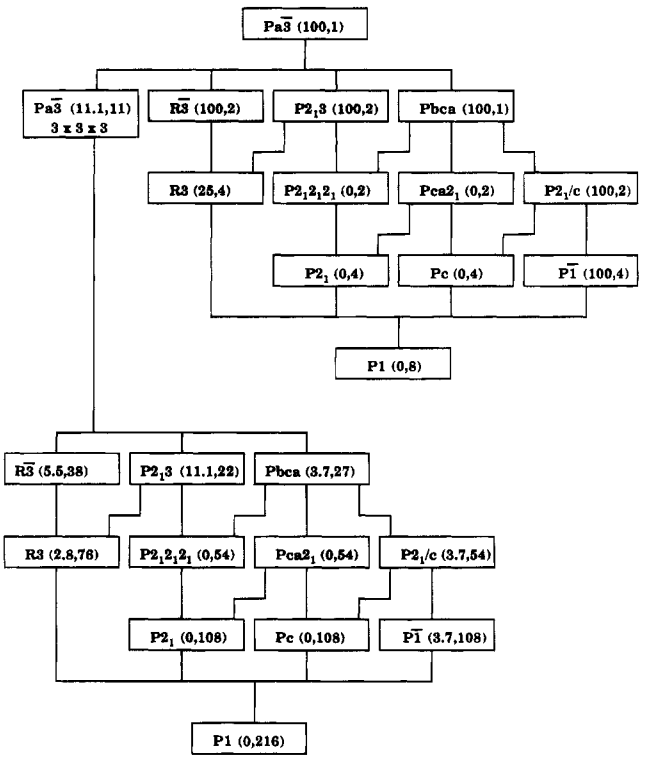

Figure 4. Possible space groups for $A^{4+}M^{5+}{}_2O_7$ compounds based on distortions of the ideal cubic structure. The first number in parentheses is the percent M−O−M linkages constrained by space group symmetry to be 180°; the second number is the number of crystallographically distinct M atoms for that space group.

to 48 and 67 °C. As x further increased, the transitions became more diffuse as indicated by a broadening and weakening of the DSC peaks. For $x = 0.3$, only one peak at about 53 °C was apparent. No DSC peaks were ever found below room temperature. A room-temperature X-ray pattern for $ZrVPO_7$ was carefully examined and found to have no superstructure reflections. The shape of the DSC peak at 290 °C for ZrP_2O_7 suggests that this transition is also first order. Results in the $HfV_{2-x}P_xO_7$ series were essentially the same as in the $ZrV_{2-x}P_xO_7$ series.

Figure 4 shows the space groups which could occur as symmetry elements are removed from the ideal cubic AM_2O_7 structure in space group $Pa\bar{3}$. The transition which apparently always occurs is the one where the cubic cell edges are tripled but the space group remains $Pa\bar{3}$. Many of the 3-fold axes and inversion centers are lost during this transition, but some remain. This transition leads to eleven crystallographically distinct sites for tetrahedral M cations. Three of the sites remain on 3-fold axes which accounts for 11% of all such cations. In the ideal structure, all oxygen atoms of the M−O−M linkage are at inversion centers on the 3-fold axes. In the supercell, most of the M−O−M angles (89%) are bent away from 180°. However, one oxygen site remains on the 3-fold axis with an inversion center. Another remains on the 3-fold axis but without an inversion center. The M−O−M angles involving oxygen atoms on 3-fold axes are required by the space group symmetry to be 180°. A description of the atomic displacements involved in the formation of the 3 × 3 × 3 superstructure is challenging. There are 134 positional parameters to consider. Structural refinements

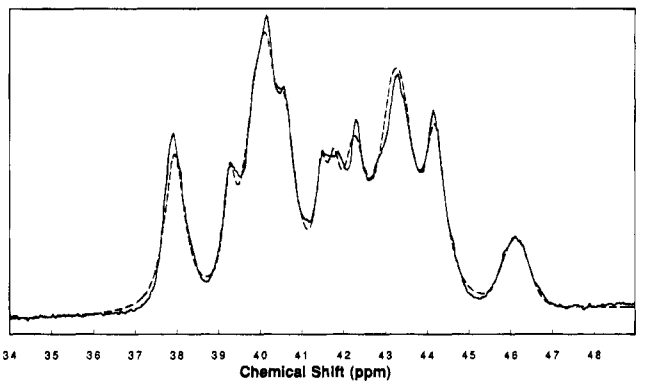

Figure 5. ^{31}P NMR MAS spectrum for ZrP_2O_7 at room temperature. The broken line represents the model of 11 mostly Lorentzian peaks and 1 Gaussian peak at 46 ppm. The MAS frequency was 18 kHz, and the chemical shift reference was phosphoric acid.

are in progress using high-resolution neutron and X-ray powder diffraction data as well as single-crystal X-ray diffraction data in the case of ZrV_2O_7. Preliminary results show that the oxygen atoms of the V−O−V or P−O−P linkages are always strongly displaced from the position required for a 180° bond angle. This may be regarded as a vibrational effect at high temperatures. However at lower temperatures where the 3 × 3 × 3 superstructure exists, this displacement is presumably static for the M−O−M linkages not on 3-fold axes but may still be dynamic for M−O−M linkages on the 3-fold axes. Details of the crystallographic studies as a function of temperature will be published elsewhere.

The proposed 3 × 3 × 3 superstructure is supported by NMR measurements. The room-temperature ^{31}P spectrum for ZrP_2O_7 at high resolution[29] is shown in Figure 5. Superimposed on the data is a least-squares fit to 11 mainly Lorentzian peaks and 1 Gaussian peak at 46 ppm. The fits to the 11 peaks include a small Gaussian admixture. Eight of these peaks were constrained to unit intensity, and three were constrained to one-third unit intensity in accordance with the $Pa\bar{3}$ space group. A preliminary fit in which the line widths of the individual peaks were free parameters showed a systematic tendency for narrower widths for the three less intense lines. In the fit shown in Figure 5, the widths of the three (intensity $^1/_3$) lines and the eight (intensity 1) lines were constrained so that the widths could vary by no more than 10% within each group. This procedure is consistent with the expectation that the line widths of closely similar sites should not vary widely. The model fits the data well and is consistent with space group $Pa\bar{3}$ and the 3 × 3 × 3 superstructure described above. Table 1 reports the chemical shift of each peak as determined by the least-squares fit. The Gaussian peak is assumed to be the result of an unknown impurity phase representing 4.4% of the total intensity. This is presumably the same phase giving rise to three weak peaks of an unidentified impurity in our neutron diffraction pattern of ZrP_2O_7.

The room temperature ^{31}P spectrum for $x = 1$ is shown in Figure 6. Two distinct lines are observed. Comparing relative intensities for the various compositions $x = 2$, 1.6, 1.0, and 0.3, we have identified the lower chemical shift line as representing phosphorus in a V−O−P bonding configuration and the high shift line as phosphorous in a P−O−P bonding configuration. The ratio of the number of V−O−P to P−O−P bonds was measured to be 0.28 and 4.37 for $x = 1.6$ and 1.0, respectively. If sites were occupied randomly, these ratios would be 0.5 and 2.0, respectively. Therefore, a mixture of P_2O_7 and V_2O_7 groups is favored over PVO_7 groups for $x = 1.6$ (phosphorous rich), whereas PVO_7 groups are favored over a mixture of P_2O_7 and V_2O_7 groups for $x = 1.0$ (equal vanadium and phosphorus content). No P−O−P bonds were observed in the $x = 0.3$ material. In the mixed materials, no structure is observed in the NMR spectra. It was not possible to resolve distinct lines for V_2O_7 and PVO_7 groups in the ^{51}V spectra at 8 T. However, spectra obtained at 11.7 T exhibited a shoulder (25 ppm) on the main ^{51}V resonance at ~5 ppm in a sample with $x = 1.0$.[29]

Figure 7 shows the ^{51}V spectra in ZrV_2O_7 at various temperatures. The systematic uncertainty in the sample temperature, due primarily to gradients in the air flow

Table 1. ^{31}P NMR Parameters for the Series $ZrV_{2-x}P_xO_7$

sample	peak	chemical shift (ppm)[a]	hwhm (ppm)	rel int
ZrP_2O_7[b]	1	37.93	0.29	1
	2	39.25	0.16	0.33
	3	39.82	0.35	1
	4	40.12	0.28	1
	5	40.57	0.30	1
	6	41.43	0.16	0.33
	7	41.73	0.18	0.33
	8	42.22	0.33	1
	9	43.07	0.35	1
	10	43.35	0.35	1
	11	44.12	0.29	1
	12	46.04	0.36	0.39
$ZrV_{0.4}P_{1.6}O_7$	V−O−P	30.63	2.7	1
	P−O−P	43.46	2.5	3.62
$ZrVPO_7$	V−O−P	29.98	2.7	4.37
	P−O−P	43.88	2.5	1
$ZrV_{1.7}P_{0.3}O_7$	V−O−P	28.73	2.4	1

[a] Referenced to phosphoric acid. [b] Peaks 1−11 are a sum of Gaussian and Lorentzian functions. The percent Gaussian intensity and ratio of Gaussian width to Lorentzian width are fit parameters but are constrained to be the same for each line. These numbers are 14.1% and 1.24%, respectively. The relative intensity of these peaks is also constrained to the fit. The width of lines with 0.33 relative intensity are allowed to float in the range 0.164 ± 0.0165. The width of lines with unit relative intensity are allowed to float in the range 0.316 ± 0.0316. Peak 12 is purely Gaussian with the intensity, width, and position allowed to float freely. The intensity of this line accounts for 4.4% of the total intensity.

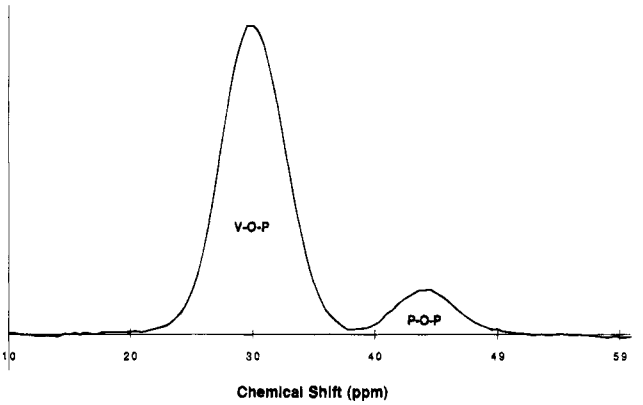

Figure 6. ^{31}P NMR spectrum for $ZrVPO_7$ at room temperature.

(29) We are indebted to Dr. Lucy Bull at the University of California, Santa Barbara for assistance in obtaining this spectrum.

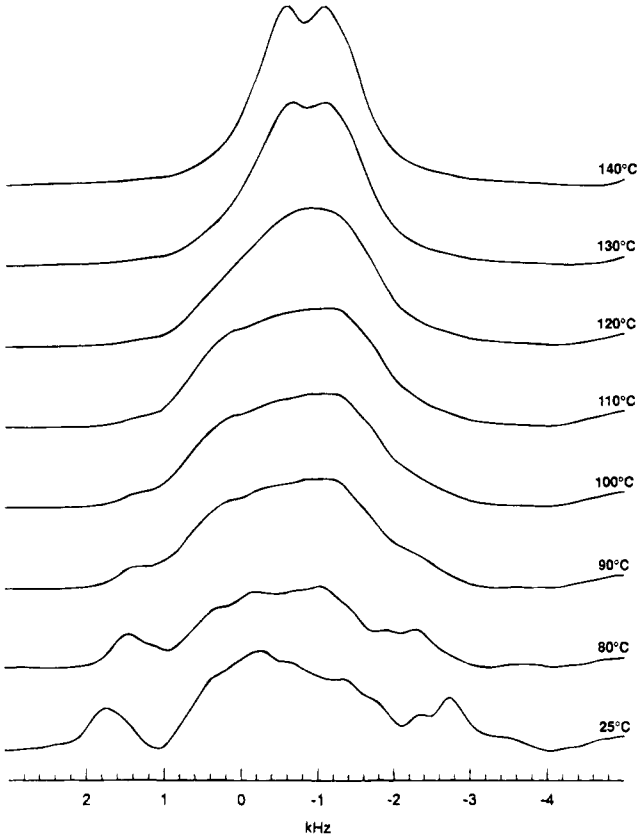

Figure 7. ^{51}V NMR spectra at various temperatures.

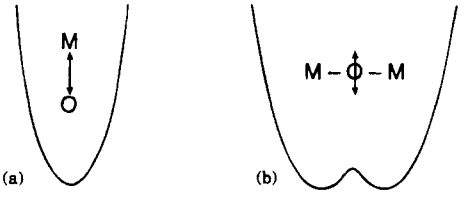

Figure 8. Schematic potential wells for M–O–M linkages. A sharp well (a) for the M–O bond along the M–O–M linkage and a broad well (b) for oxygen perpendicular to this linkage.

system and calibration errors, is estimated to be ±5 °C. It can be seen that evidence of the 3 × 3 × 3 superstructure remains at 80 °C, but this structure is washed out in the 90 °C spectrum, consistent with a phase transition in this temperature range. A transition in the 90–110 °C range is not apparent in the NMR spectra, but a gradual narrowing of the line indicates a single quadrupole-split site at temperatures above 130 °C. The 507 Hz splitting in the high-temperature spectrum is characteristic of an axially symmetric quadrupole powder pattern and is consistent with observed first-order quadrupole satellite transitions. A value of the nuclear quadrupole coupling constant, e^2qQ/h, 1.92 MHz was determined from the satellite splitting. Within experimental uncertainty, e^2qQ/h is independent of temperature in the range 25–180 °C.

Discussion

Contraction, rather than expansion, with increasing temperature can apparently be caused by different structural features for different materials. In most cases of negative volume expansion, the normal positive thermal expansion of chemical bonds in some directions actually causes lattice contraction in other directions. Such materials are then highly anisotropic in their thermal expansion properties. The net effect can be a very low volume thermal expansion which can be slightly negative. An alternate explanation must be sought for isotropic compounds showing negative thermal expansion.

It is well-known that at low temperatures the O–O distance in CO_2 decreases with increasing temperature due to the bending mode in this molecule. Likewise, metal–oxygen–metal (M–O–M) units are susceptible to a decrease in the M–M distance with increasing temperature when the M–O–M angle is close to 180° and other conditions are met. Most important is that the M–O bond be highly covalent. This has two intimately related consequences. One is that the thermal expansion of the M–O bond will be very small; the other is that thermal motion of oxygen will be very small along the direction of the M–O bonds. The thermal motion of oxygen perpendicular to M–O–M must be relatively high, and this normally occurs. A special case exists where the lattice symmetry requires that the M–O–M bond angle be 180°. Such an angle is generally not favorable, and this 180° instability is usually attributed to the cost of sp hybridization for oxygen.

Schematic potential wells for the 180° M–O–M linkage are shown in Figure 8. The well is sharply defined for interactions along the M–O–M linkage but is very broad for interactions perpendicular to the linkage. The bump in the middle of the broad maximum is due to the instability of the 180° bond angle for the M–O–M linkage. A consequence of the broad potential well (Figure 8b) is that M–O–M bond angle is likely to deviate strongly from 180° at high temperatures at any instant in time. With increasing temperature, maintaining the appropriate M–O distance causes the M–M distance to decrease. If the M–O–M linkage only occurs in one direction, negative thermal expansion would be expected only in that direction. In the case of the cubic $A^{4+}M^{5+}{}_2O_7$ family, the M–O–M linkages occur along all three dimensions due to the cubic symmetry. The negative thermal expansion is therefore isotropic.

In structures containing a linear M–O–M linkage with oxygen in only 2-fold coordination, a common phenomenon with decreasing temperature is a phase transition to lower symmetry where the M–O–M angle is no longer required to be 180°. In other words, the vibrating oxygen becomes trapped on one side of the maximum in Figure 8b. This situation occurs, for example, in the perovskite structure. The M–O–M angles in AMO_3 perovskites are ideally 180°. Many perovskites have this ideal cubic symmetry at high temperatures, but a lattice distortion frequently occurs as temperature decreases. The instability of the 180° M–O–M bond angle causes the MO_6 octahedra to tilt during these distortions. In the common orthorhombic distortion of the perovskite structure, all M–O–M angles have bent away from 180°, and this results in an increase in the primitive unit cell from 1 to 4 formula units. This is in marked contrast to the increase of unit cell contents of cubic $A^{4+}M^{5+}{}_2O_7$ compounds from 4 to 108 formula units when some of the M–O–M bonds bend to form the 3 × 3 × 3 superstructure.

A major question to be addressed is why the 3 × 3 × 3 superstructure is preferred over the other possibilities indicated in Figure 4. In particular, space groups

$P2_12_12_1$, $Pca2_1$, $P2_1$, Pc, and $P1$ all offer the possibility of completely relaxing the 180° M−O−M angle constraint without any increase in the size of the unit cell. It would seem that although these space groups allow for local relaxation of the 180° M−O−M linkage, they apparently do not allow for this to occur in a cooperative, ordered manner without severe distortion of the AO_6 and/or MO_4 polyhedra. To test this hypothesis, modeling was conducted in the appropriate space groups using DLS.[30] In this approach, the AO_6 octahedron and MO_4 tetrahedron are semirigid, but O−A−O and O−M−O angles are less restrained than A−O and M−O distances. The A−O−M and M−O−M linkages are considered to be highly flexible, but cation−cation distances are not allowed to become unacceptably short. The R value is the least-squares refinement of DLS is defined as $R = \sqrt{\sum(w \cdot \delta d)^2/\sum(w \cdot d)^2}$, where d is an A−O, M−O, or O−O distance, δd is the difference between the prescribed and actual distance, and w is a weighting factor. After many calculations to assure that the global minima had been obtained, the R values were 10.1% for $Pca2_1$, 9.6% for $P2_12_12_1$, 8.7% for both $P2_1$ and Pc, and 7.9% for $P1$. A much better fit with prescribed distances and angles ($R = 2.0\%$) was obtained with the $3 \times 3 \times 3$ superstructure in space group $Pa\bar{3}$. However, in this model the 11.1% of the M−O−M linkages that are constrained by symmetry to be 180° are actually assumed to be bent in a random manner.

The ideal $A^{4+}M^{5+}{}_2O_7$ structure (Figure 1) apparently always partially relieves the 180° M−O−M angle instability by adopting the cubic $3 \times 3 \times 3$ superstructure. This occurs despite that fact that distortions to orthorhombic $P2_12_12_1$ or $Pca2_1$, for example, might have been expected to relieve all the 180° M−O−M angle instabilities without any increase in the primitive unit cell, and the number of crystallographic M atoms increases only to two (Figure 4). Once the cubic $3 \times 3 \times 3$ superstructure has formed, it becomes very difficult to remove the remaining 180° M−O−M instabilities (Figure 4). Distortions to orthorhombic $P2_12_12_1$ or $Pca2_1$ might relieve the instabilities, but then 54 crystallographically distinct M sites would be created.

The apparent inability of the cubic $A^{4+}M^{5+}{}_2O_7$ structure to distort a structure with M−O−M linkages bent away from 180° in a completely ordered fashion indicates that this basic structure is not thermodynamically stable at low temperatures. This suggests that there may be a completely different structure for such compounds as the low-temperature stable phase. This structure may have been found for ZrP_2O_7. There is a report[31] of a high-pressure form of ZrP_2O_7 which is 15.7% denser than the cubic form at ambient conditions. Unfortunately, the structure of this high-pressure form has not been determined. However, it was observed that this high-pressure phase did not convert to the cubic structure on heating for 65 h at 600 °C. This suggests the possibility that the more dense phase is also the low-temperature modification of ZrP_2O_7. At 1000 °C, the high-pressure form quickly converts to the cubic form, which is presumably the stable form at that temperature.

Phase transitions involving a change from linear to nonlinear M−O−M linkages normally occur at temperatures well above room temperature. For example, in the various forms of crystalline silica, these transitions are in the range 260−575 °C.[32] For quartz, cristobalite, and tridymite the situation is much like that for the ZrP_2O_7 family of compounds. Below the SiO_2 phase transitions, the thermal expansion is positive and could be considered to be normal. Above the transitions, the thermal expansion becomes very low. At temperatures above 1000 °C, the thermal expansion becomes negative. This behavior can be qualitatively rationalized with the potential wells shown in Figure 8. The phase transition bending the M−O−M linkage away from 180° occurs at a lower temperature in ZrV_2O_7 and HfV_2O_7 than in any other known oxide. This is likely due to the low lying 3d orbitals of vanadium which can be used for π bonding. Just as π bonding can stabilize a 180° bond angle in CO_2, π bonding can be a significant factor diminishing the instability associated with a 180° angle for the V−O−V linkage. The second phase transition in the vanadates, which is not known to occur in the AM_2O_7 phosphates, may also be related to the π bonding in the vanadates. Furthermore, the exceptionally large negative thermal expansion found for ZrV_2O_7 and HfV_2O_7 from about 150 to 750 °C may be related to the greater polarizability of a system with low-lying d orbitals.

The depression of the temperature of the phase transition in the $ZrV_{2-x}P_xO_7$ solid solution series relative to both end members might be considered as a normal solid solution effect, analogous to freezing point depression. In this explanation, the disorder inherent in any solid solution interferes with the long-range cooperative forces required for the phase transition. However, another explanation is possible for this series. We know that the solid solution cannot be well represented as $Zr(V_2O_7)_{1-x}(P_2O_7)_x$ because of the presence of VPO_7 groups. On the basis of our ^{31}P NMR results, the structural formula for $ZrVPO_7$ would be $Zr(PVO_7)_{0.68}(P_2O_7)_{0.16}(V_2O_7)_{0.16}$. The instability of a linear P−O−V linkage is unknown relative to the instabilities of linear P−O−P and V−O−V linkages. Therefore, the depression of the phase transitions in the $ZrV_{2-x}P_xO_7$ series might be in part due to the presence of the P−O−V linkages.

Acknowledgment. This work was supported in part by the Oregon Metals Initiative which is funded through a partnership with the Oregon Economic Development Department, the Oregon Lottery, the Oregon Joint Graduate Schools of Engineering, and Teledyne Wah Chang Albany. We wish to express our appreciation to Dr. Randy Lundquist for assistance with the least-squares fit shown in Figure 5. Work of N.R., R.D., and W.W.W. was supported in part by NSF DMR-9305780.

CM940458Y

(30) Meier, W. M.; Villiger, H. *Z. Kristallogr.* **1966**, *129*, 161.
(31) Sclar, C. B.; Carrison, L. C.; Schwartz, C. M. *Nature* **1964**, *204*, 573.
(32) Taylor, D. *Br. Ceram. Trans. J.* **1984**, *83*, 129.